1-1-2015

Electronic structure and photocatalytic water oxidation activity of RTiNO2 (R = Ce, Pr and Nd) perovskite nitride oxides

Spencer H. Porter
University of Wollongong, sp733@uowmail.edu.au

Zhenguo Huang
University of Wollongong, zhenguo@uow.edu.au

S X. Dou
University of Wollongong, shi@uow.edu.au

Samantha Brown-Xu
Ohio State University

Md. Golam Mahabub Sarwar
University of Wollongong, mgms225@uowmail.edu.au

See next page for additional authors

Electronic structure and photocatalytic water oxidation activity of RTiNO2 (R = Ce, Pr and Nd) perovskite nitride oxides

Abstract

Three perovskite nitride oxides $CeTiNO_2$, $PrTiNO_2$, and $NdTiNO_2$ have been synthesized and their electronic structures and photocatalytic activities characterized and compared to $LaTiNO_2$. All three compounds have band gaps that fall in the range 2.0 − 2.1 eV, very similar to $LaTiNO_2$, which enables them to absorb a significant fraction of the visible spectrum. Photocatalytic oxygen evolution studies under visible light irradiation in the presence of a sacrificial electron acceptor (Ag^+) show that the activity of $NdTiNO_2$ (16 μmol/g/hr) is comparable to that of $LaTiNO_2$ (17 μmol/g/hr), while $PrTiNO_2$ (11 μmol/g/hr) and $CeTiNO_2$ (5 μmol/g/hr) have activities that are only 65% and 30% that of $LaTiNO_2$. X-ray photoelectron spectroscopy measurements reveal the presence of partially occupied f-orbital states that lie in the band gap for $CeTiNO_2$, and near the valence band maximum for $PrTiNO_2$. As evidenced by time resolved IR kinetic decay, these localized f-orbital states act as electron-hole recombination centers that inhibit the photocatalytic activities of both compounds. On the other hand, $NdTiNO_2$, where the f-orbital energies fall below the valence band maximum, does not suffer from this effect.

Keywords

water, photocatalytic, structure, electronic, rtino2, activity, r, oxidation, ce, pr, nd, perovskite, nitride, oxides

Disciplines

Engineering | Physical Sciences and Mathematics

Publication Details

Porter, S. H., Huang, Z., Dou, S., Brown-Xu, S., Sarwar, A. Golam., Myers, R. C. & Woodward, P. M. (2015). Electronic structure and photocatalytic water oxidation activity of *R*$TiNO_2$ (*R* = Ce, Pr and Nd) perovskite nitride oxides. Chemistry of Materials, 27 (7), 2414-2420.

Authors

Spencer H. Porter, Zhenguo Huang, S X. Dou, Samantha Brown-Xu, Md. Golam Mahabub Sarwar, Roberto C. Myers, and Patrick M. Woodward

Electronic structure and photocatalytic water oxidation activity of $RTiNO_2$ (R = Ce, Pr and Nd) perovskite nitride oxides

Spencer H. Porter[†], Zhenguo Huang[†,*], Shixue Dou[†], Samantha Brown-Xu[#], A.T.M. Golam Sarwar[%], Roberto C. Myers[%], Patrick M. Woodward [#,*]

[†]Institute for Superconducting and Electronic Materials, University of Wollongong, Wollongong, NSW 2500, Australia

[%]The Ohio State University, Dept. of Electrical and Computer Engineering, Columbus, OH 43210

[#]The Ohio State University, Dept. of Chemistry & Biochemistry, Columbus, OH 43210

KEYWORDS: Titanium, nitride oxide, oxynitride, perovskite, photocatalysis, water-splitting, water oxidation

ABSTRACT: Three perovskite nitride oxides $CeTiNO_2$, $PrTiNO_2$, and $NdTiNO_2$ have been synthesized and their electronic structures and photocatalytic activities characterized and compared to $LaTiNO_2$. All three compounds have band gaps that fall in the range 2.0 − 2.1 eV, very similar to $LaTiNO_2$, which enables them to absorb a significant fraction of the visible spectrum. Photocatalytic oxygen evolution studies under visible light irradiation in the presence of a sacrificial electron acceptor (Ag^+) show that the activity of $NdTiNO_2$ (16 μmol/g/hr) is comparable to that of $LaTiNO_2$ (17 μmol/g/hr), while $PrTiNO_2$ (11 μmol/g/hr) and $CeTiNO_2$ (5 μmol/g/hr) have activities that are only 65% and 30% that of $LaTiNO_2$. X-ray photoelectron spectroscopy measurements reveal the presence of partially occupied f-orbital states that lie in the band gap for $CeTiNO_2$, and near the valence band maximum for $PrTiNO_2$. As evidenced by time resolved IR kinetic decay, these localized f-orbital states act as electron-hole recombination centers that inhibit the photocatalytic activities of both compounds. On the other hand, $NdTiNO_2$, where the f-orbital energies fall below the valence band maximum, does not suffer from this effect.

1. Introduction

Visible light driven photocatalytic water splitting has attracted considerable attention as an attractive approach to harvesting solar energy. Instead of converting the energy of solar radiation to electrical energy, water splitting produces chemical energy in the form of H_2 and O_2. The photocatalytic process of generating these gases can be broken down into two half reactions—water oxidation by photogenerated holes to produce O_2, and water reduction by photogenerated electrons to produce H_2.

Despite four decades of research a photocatalyst that can efficiently split water when irradiated with only visible light remains elusive. A promising way to address this challenging problem is to use separate photocatalysts to drive each half-reaction and couple these two through a redox-active shuttle in the so-called Z-scheme approach. For the water oxidation half of the Z-scheme approach, the most widely studied photocatalysts are oxides like $BiVO_4$ (E_g ~ 2.4 eV)[1-4] and WO_3 (E_g ~ 2.4 eV).[5-8] While the band gaps of these oxides are small enough to absorb visible light, they are still large enough that a significant fraction of the visible spectrum is not harvested.

In recent years the nitride oxide class of compounds, commonly referred to as oxynitrides, have been identified as promising photocatalysts. Nitride oxides benefit from a reduced band gap with respect to analogous oxides because the valence band maximum (VBM) shifts up in energy due to the presence of nitrogen 2p states which are more electropositive than the oxygen 2p states that comprise the valence band in most oxide photocatalysts.[9] TaON (E_g = 2.4 eV) was one of the first mixed anion compounds reported for water oxidation.[10,11] Recently $BaNbNO_2$ (E_g = 1.7 eV)[12] and $LaTiNO_2$ (E_g = 2.1 eV)[13] have been shown to possess excellent O_2 evolution rates, and hence are attractive candidates for the oxygen evolution photocatalyst in a Z-scheme setup.

Motivated by the best-in-class performance and high quantum efficiency of $LaTiNO_2$ we have prepared three related nitride oxide perovskites, $RTiNO_2$ (R = Ce, Pr, Nd), and characterized their electronic structures and oxygen evolution photocatalytic activities. The synthesis and structural characterization of these compounds have previously been reported,[14-17] but their optical, electronic and photocatalytic properties have not been studied. To put the properties of these three nitride oxide perovskites in context we have also prepared and characterized $LaTiNO_2$ for comparison.

2. Experimental

Samples were prepared by a solid state ammonolysis route from $R_2Ti_2O_7$ precursors. Stoichiometric amounts of TiO_2 (99.9%, GFS Chemicals) and the appropriate oxide or hydroxide of the rare earth cation ($La(OH)_3$: 99.99%, GFS Chemicals; Pr_6O_{11}: 99.999%, Cerac; CeO_2: 99.90%, Acros; Nd_2O_3: 99.9%, Alfa) were ground together using a mortar and pestle for 30 min. Precursors were synthesized in air (La and Nd) or 5% H_2/N_2 gas (Pr and Ce) in platinum boats at 1200 °C for 8 hr with a 5 °C ramp/cool rate. Alumina boats containing the precursors were

placed in a tube furnace and gaseous ammonia was flowed over the sample during annealing. The furnace was ramped at 10 °C/min to 950 °C, held for 20 hr, and then cooled at 10-20 °C/min to room temperature. This annealing cycle was repeated four times with intermittent grinding.

LECO High Temperature NO Elemental Combustion Analysis was performed to determine the nitrogen to oxygen ratio. The purity of each compound was assessed through Rietveld refinements on powder X-ray diffraction data obtained from a Bruker D8 Advance diffractometer (Ge monochromator, 10 – 110° 2θ, 0.015° step size, and 1 s dwell time). Rietveld refinements were performed using GSAS with the EXPGUI interface.[18] Isotropic displacement parameters were used for all ions.

The Brunauer−Emmett−Teller (BET) surface area and pore volume of the samples were measured by a Micromeritics Accelerated Surface Area and Porosimetry (ASAP) 2020 instrument, using nitrogen adsorption/desorption isotherms collected at liquid nitrogen temperature. The desorption branch of the isotherm was used to determine the Barret−Joyner−Halenda (BJH) pore size distribution. Before the measurement, the samples were degassed for 12 hr at 130 °C under a vacuum better than 2 μm Hg.

Scanning electron microscopy (SEM), for sample imaging, and electron dispersive X-ray spectroscopy (EDXS), for chemical composition analysis, were performed in a Zeiss Ultra 55 Plus FE-SEM with an electron accelerating voltage of 15 kV. Samples were prepared by dispersing the particles on a conductive carbon tab mounted on a metal substrate holder.

X-ray photoelectron spectroscopy (XPS) measurements were performed on powders anchored in carbon tape using a Kratos Axis Ultra XPS instrument. The photoelectron excitation processes were initiated using an Al Kα source (energy 1486.6 eV). The vacuum in the analysis chamber was maintained at 1×10^{-9} Torr. Binding energy reference for all samples was set to the C 1s peak, 284.5 eV. UV-visible diffuse reflectance data were collected using an Ocean Optics USB4000-UV-Vis spectrometer equipped with a standard reflectance probe and a DH-2000-BAL deuterium/tungsten halogen light source. Data were generated using SpectroSuite software, then transformed by the Kubleka-Munk method for subsequent interpretation.

The femtosecond time-resolved infrared (TRIR) experiment was performed using a Coherent Ti:sapphire oscillator and regenerative amplifier combination (1 kHz, 50 fs FWHM). The 800 nm output is split and used to generate the mid-IR probe and visible pump beams. For the probe, an OPerA optical parametric amplifier (OPA) with a difference frequency generation (DFG) attachment produces mid-IR energies ranging from 2500 – 800 cm^{-1}. A Ge beamsplitter is used to produce a probe and a reference IR beam that pass through the sample with ~ 5 mm separation. The pump beam is also generated from an OPA with a UV/vis or DFG attachment, after which it passes through a delay stage and is overlapped with the probe at the sample. Probe and reference spectra were collected on a Triax 320 spectrometer equipped with a HgCdTe array (2 × 32) detector.[19] Samples were prepared by uniaxially pressing 2 wt. % *R*$TiNO_2$ in KBr (totaling 400 mg) into a pellet at 100 MPa. The samples were excited at 600 nm, near the band edges (620 to 590 nm), with an energy of 1.0 – 1.5 μJ at the sample. Spectra were background subtracted, plotted, and analyzed using Origin. The kinetic profiles were fit using a triple exponential equation of the form

$$S(t) = \Sigma_i A_i e^{-t/\tau_i} + C \quad (1)$$

where A_i is the amplitude, τ_i is the lifetime, and C is an offset. Errors in the lifetimes are reported as standard errors of the exponential fits.

For photocatalytic measurements, the surface of the oxide nitrides was wet impregnated with a CoO_x co-catalyst from 2 wt. % $Co(NO_3)_2{\cdot}6H_2O$ (>99.0%, Baker) using a method previously described.[13] Water oxidation half reactions were executed in a closed, top-irradiated quartz vessel. 100 mg of co-catalyzed nitride oxide powder and 100 mg La_2O_3 (99.99%, GFS Chemicals) (as a pH buffer) were added to 100 mL of a 0.05 M $AgNO_3$ aqueous solution and suspended using a magnetic stirrer. The $Ag^+(aq)$ ions act as a sacrificial electron acceptor. Reactant solutions were purged of air by bubbling argon through the system until the background GC spectra were featureless. Visible light irradiation was performed using a 150 W Xe lamp equipped with a 400 nm long pass filter and a cold mirror (Newport Oriel, Stratford, CT, USA; optical power: 26μW/cm^2). Gases evolved were separated by a Shimadzu GC-14A gas chromatograph equipped with a 60/80 molecular sieve 5A (Sigma Aldrich, St. Louis, MO, USA) and a thermal conductivity detector. These runs were calibrated against an external standard curve for oxygen.

A known oxygen evolving catalyst, $LaTiNO_2$, was used as a benchmark for comparison. To ensure that the system is visible light active only, a UV active perovskite photocatalyst, $SrTiO_3$, was tested for O_2 evolution. The $SrTiO_3$ sample was prepared from TiO_2 (99.9%, GFS Chemicals) and $SrCO_3$ (99.99%, Alfa) by two cycles of heating to 1000 °C, holding for 8 hr each time (with intermittent grinding). Quantum efficiency measurements on $LaTiNO_2$ and $NdTiNO_2$ were carried out using O_2 evolution (same experimental and instrumental set-up) under 450 nm band pass filtered 150W Xe arc lamp light calibrated by a Si photodiode (Thor labs, Newton, NJ, USA).

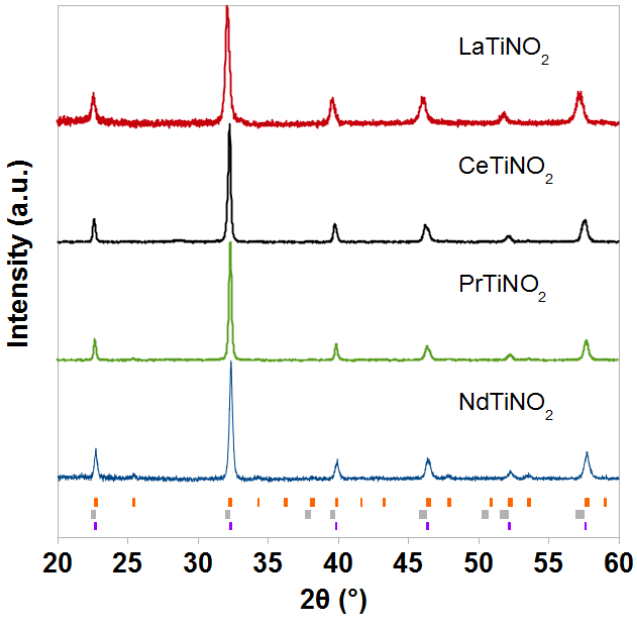

Figure 1. Laboratory XRD patterns of *R*$TiNO_2$ from 20º to 60º 2θ. Reflection positions for a simple cubic perovskite ($Pm\bar{3}m$) with lattice parameter a_p, a triclinic perovskite ($I\bar{1}$) with $\sqrt{2}a_p \times 2a_p \times \sqrt{2}a_p$ lattice parameters, and an orthorhombic perovskite (*Pnma*) with $\sqrt{2}a_p \times 2a_p \times \sqrt{2}a_p$ lattice parameters, are shown with purple (lower), gray (middle), and orange (upper) hash marks, respectively.

3. Results & Discussion

3.1 Composition and structure

Combustion analysis carried out on the *R* = Ce, Pr compounds gives compositions of $CeTiN_{0.99(3)}O_{2.01(3)}$ and $PrTiN_{1.03(3)}O_{1.97(3)}$. These results indicate an anion stoichiometry that matches the nominal composition, within experimental error, and confirms the 3+ oxidation state assignment for the rare-earth ion.

The structures of the $RTiNO_2$ (*R* = La – Nd) phases have been reported elsewhere using NPD.[14,17] XRD powder patterns (Figure 1) were refined in their reported space groups, *Pnma* for $RTiNO_2$ (R = Ce, Pr, Nd) and $I\bar{1}$ for $LaTiNO_2$. Lattice parameters for all four compounds were determined using whole pattern fitting of the XRD powder patterns, and are shown in Table 1. The compounds are phase pure and have space group symmetry and lattice parameters that are in agreement with the previously reported values.

Table 1. Lattice parameters for Rietveld refined $RTiNO_2$ (*R* = La, Ce, Pr, Nd) perovskites.

	$LaTiNO_2$	$CeTiNO_2$	$PrTiNO_2$	$NdTiNO_2$
Space group	*I*1	*Pnma*	*Pnma*	*Pnma*
a (Å)	5.592(8)	5.5563(4)	5.531(1)	5.541(1)
b (Å)	7.870(5)	7.8017(4)	7.7895(5)	7.796(1)
c (Å)	5.582(6)	5.5349(3)	5.5355(9)	5.526(1)
α (Å)	90.1(2)	90	90	90
β (Å)	90.18(5)	90	90	90
γ (Å)	90.3(2)	90	90	90
V (Å^3)	245.69(9)	239.93(3)	238.49(3)	238.74(5)

3.2 Surface properties

A type-II adsorption isotherm has been observed for $PrTiNO_2$ as shown in Figure 2 (see Supporting Information for the iostherms of the other compounds). This isotherm is common for vapor adsorption, *e.g.* water vapor adsorbed on a hydrophobic material. The specific surface areas for $RTiNO_2$ determined by BET at 77 K are 4 – 6 $m^2 \cdot g^{-1}$. Capillary condensation driven volume increases in the adsorption branch, occur at relatively high pressure (~ $P/P_o > 0.9$), which is indicative of large pore diameter. The pore size distribution (inset in Figure 3), determined from the corresponding desorption branch using the BJH method, is broad with pore volume increasing as pore diameter decreases. A wide distribution of pore diameters exists in the range of 20 – 90 nm. These compounds have comparable surface area, pore volume, and pore size (Table 2), which is not unexpected given the identical solid state ammonolysis used for the synthesis. The high temperature and long dwell time allow for considerable grain growth and grain boundary minimization, which lead to small surface area and pore volume.

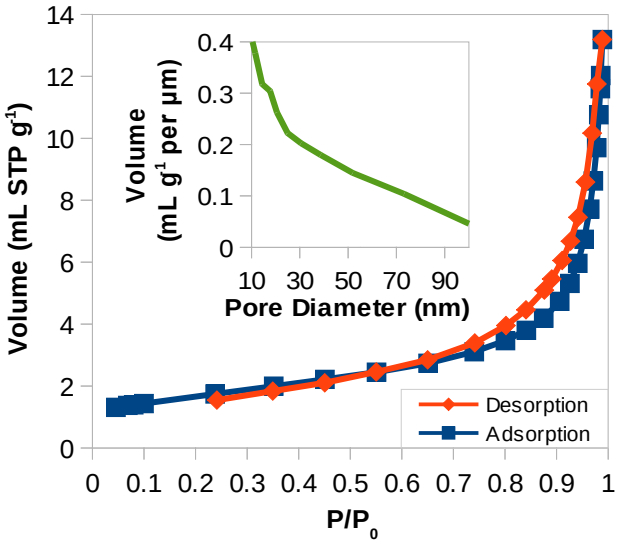

Figure 2. N_2 isotherm and pore size distribution (inset) for $PrTiNO_2$

Table 2. Surface features of $RTiNO_2$ (*R* = La, Ce, Pr, Nd) powders prepared by solid state ammonolysis.

Sample:	$LaTiNO_2$	$CeTiNO_2$	$PrTiNO_2$	$NdTiNO_2$
BET Surface area (m^2/g):	6	4	6	5
Pore Volume (cm^3/g):	0.03	0.02	0.02	0.02
Mean Pore Diameter (nm):	20	18	13	17

SEM images ($NdTiNO_2$, Figure 3; $RTiNO_2$ (*R* = La – Pr), Supporting Information, Figure S4 – S6) reveal that particle size distribution is consistent across all samples. The crystal size in $CeTiNO_2$ (1 – 3 µm) is slightly larger than the other compounds, which is reflected in the BET surface area. Each sample contains both large (50 – 100 µm; not pictured) and small (100 nm – 10 µm) particles. The broad distribution of particle sizes is the result of agglomeration during annealing due to sintering. No uniform crystal habit is apparent, with a random orientation of exposed facets for all $RTiNO_2$. These observations are in-line with the results from our prior work on the same compounds, where TEM analysis shows polycrystallinity even for the smallest particles.[17] EDXS confirms that the CoO_x co-catalyst by has been uniformly distributed on the surface of $RTiNO_2$ particles.

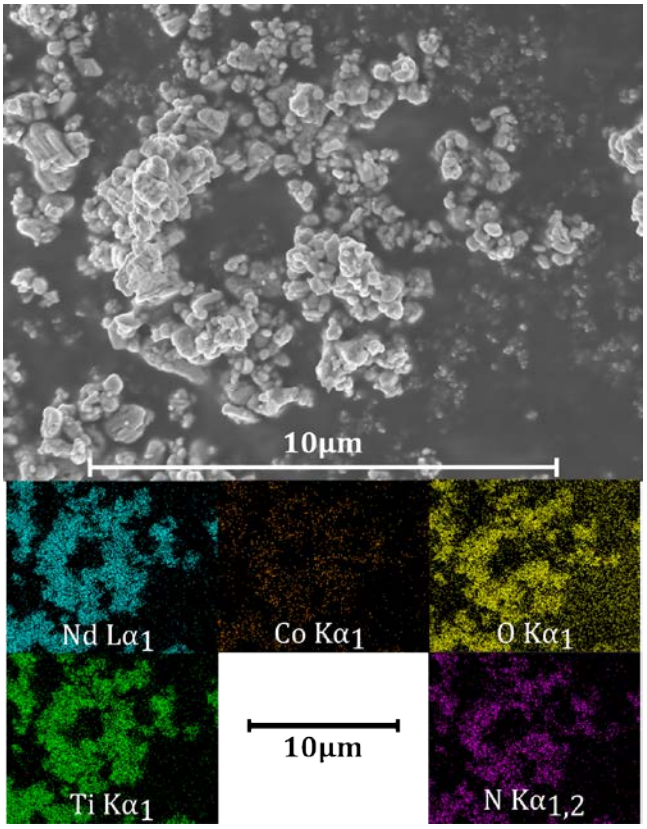

Figure 3. SEM image and EDX mapping for $NdTiNO_2$.

3.3 X-ray photoelectron spectroscopy

To evaluate the relative positions of the partially filled 4f electron energy levels, XPS measurements in the valence band photoemission region have been performed (Figure 4). The spectra of RTiNO$_2$ are characterized by strong, broad peaks spanning from 0 to 8 eV originating largely from the anion 2p orbitals that make up the valence band. A peak originating from occupied f-orbitals, and marked with a purple plus sign, is visible above the valence band edge in $CeTiNO_2$. This same peak appears as a shoulder on the anion 2p valence band edge for $PrTiNO_2$. The peak associated with 4f orbitals cannot clearly be made out in the $NdTiNO_2$ spectrum. This indicates a further shift toward higher binding energy, which implies that the position of the occupied 4f levels lies below the valence band maximum and overlaps with states well within the valence band.

The trend of increasing binding energy of the f-orbital states on going from Ce → Pr → Nd is consistent with expectations based on effective nuclear charge. Similar XPS trends have been observed in the RTaO$_4$ series.[20] Differences in crystal structure that lead to different band dispersions make a direct comparison of the RTaO$_4$ and RTiNO$_2$ XPS spectra difficult, but some qualitative comparisons can be made. In both the RTaO$_4$ and the RTiNO$_2$ series the peak associated with the occupied Ce 4f-states lies at a binding energy that is ~1 eV higher than the peak associated with the Pr 4f-states. A close inspection also reveals that the Pr 4f-states are located closer to the top of the anion 2p valence bands in $PrTiNO_2$ than in $PrTaO_4$, an effect that can be attributed to the contribution of the nitrogen 2p orbitals to the valence band of the former compound.[21] The key point is that only the more electropositive rare-earth ions (Ce and Pr) have partially filled 4f states that are at energies higher than or comparable to the valence band maximum. As seen below this feature of the electronic structure has important implications for the photocatalytic activity.

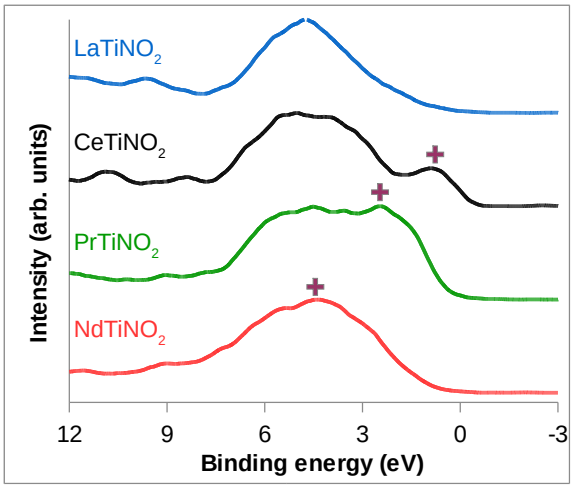

Figure 4. XPS of RTiNO$_2$ (R = La, Ce, Pr, Nd). Crosses mark the positions of the 4f states.

3.4 Time-resolved IR measurements

It has been shown previously that wet-impregnated co-catalysts significantly increase the carrier lifetimes in $LaTiNO_2$.[13] To minimize variables and examine intrinsic effects, femtosecond TRIR spectra were recorded on bare RTiNO$_2$ (Supporting Information, Figure S7 – S10) to probe the free carriers and lifetimes. In each case, the spectra display an instantaneous rise of a broad mid-IR band, though for $LaTiNO_2$ there is a slower growth component (~ 2 ps). Kinetic decay for each compound (Figure 5) is fit by a triple exponential function (Equation 1), revealing free carrier lifetimes that range from 0.59 ps to 1.1 ns (Table 3). For all RTiNO$_2$, residual signal remains at the time limit of the experiment (3 ns) indicating a slow fourth decay component, that in similar studies of TiO_2 has been attributed to defects.[22] In-line with previous photocurrent and time-resolved diffuse reflectance measurements for $LaTiNO_2$,[23] we observe relatively long lifetimes and slow recombination for $LaTiNO_2$.

The broad mid-IR signals are attributed to absorptions of free carriers within the conduction band of each material. The concentrations in $CeTiNO_2$ and $PrTiNO_2$ diminish rapidly to levels similar to or less than that of $NdTiNO_2$ beyond ~25 ps. These rapid decays are associated with the fast component (τ_1) and are presumed to decay on too short of a time scale to have any significant effect on other processes. In $LaTiNO_2$ the concentrations persist and decay more slowly.

The highly localized nature of the 4f orbitals and their location near the VB edge in $CeTiNO_2$ and $PrTiNO_2$ (see Section 3.3), can potentially act as a favorable pathway for carrier recombination. The lifetimes for $CeTiNO_2$ are particularly short. On the other hand, the 4f orbitals in $NdTiNO_2$ are located further from the VB edge where the concentration of photogenerated holes is expected to be highest. This difference could lead to reduced rates of electron-hole recombination, longer lifetimes, and allow for carriers to partake in other phenomena (such as water oxidation, see below). The slow components (τ_2 and τ_3) and

their associated longer-lived lifetimes are ordered La > Nd > Pr > Ce, validating this hypothesis.

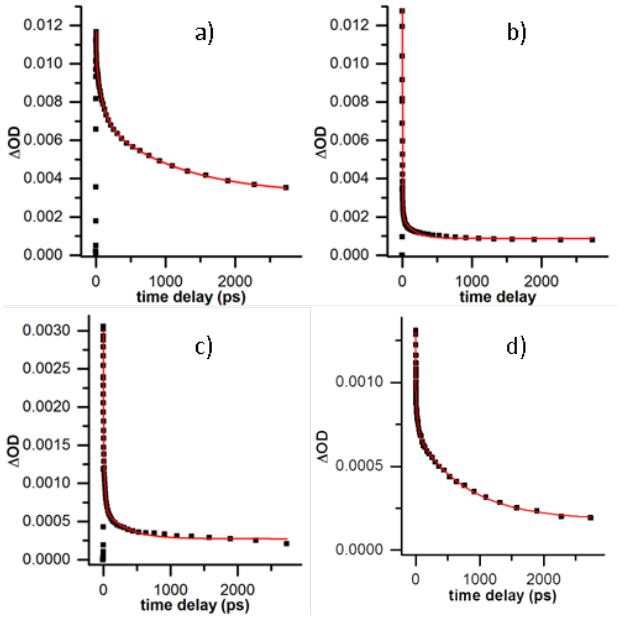

Figure 5. Kinetic traces of RTiNO$_2$ (R = a) La, b) Ce, c) Pr, d) Nd)

Table 3. Amplitudes, decay lifetimes and time of ΔOD_{max} from TRIR kinetics for RTiNO$_2$ (R = La-Nd).

	LaTiNO$_2$	CeTiNO$_2$	PrTiNO$_2$	NdTiNO$_2$
A_1	0.00607 (46%)	0.00747 (50%)	0.00130 (42%)	0.00837 (91%)
τ_1 (ps)	4.0(2)	0.59(1)	2.2(1)	1.6(1)
A_2	0.00316 (24%)	0.00647 (43%)	0.00138 (45%)	0.00027 (3%)
τ_2 (ps)	96(4)	6.7(6)	21(2)	34(4)
A_3	0.004 (30%)	0.00110 (7%)	0.00039 (13%)	0.00052 (6%)
τ_3 (ps)	1110(60)	170(20)	330(60)	798(53)
ΔOD_{max} (ps)	1.86	0.133	0.387	0.153

3.5 Optical properties

Diffuse reflectance spectra that enable quantitative comparison of the optical band gaps of LaTiNO$_2$ and the three compounds studied here are shown in Figure 6. The band gaps, which were estimated by the linear extrapolation of the adsorption onset (the Shapiro method),[25] were found to be 2.1(2), 2.0(2), 2.0(2) and 2.1(2) eV for LaTiNO$_2$, CeTiNO$_2$, PrTiNO$_2$, and NdTiNO$_2$, respectively. The band gap of LaTiNO$_2$ agrees well with previous reports.[26] The observed colors for La → Nd are red, brown-red, dark brown, and brown. The variations in color are largely due to differences in sub-band gap absorptions. The absorption coefficient for the compounds was not measured but assumed to be unique for each R cation. It is acknowledged that this could have a non-negligible impact on the photocatalytic activity. The difference in the absorption coefficients for the individual RTiNO$_2$ compounds at energies greater than the band gap should be minimal because they have very similar crystal and electronic structure.

It is well established that the valence to conduction band transitions involve transfer of an electron from crystal orbitals that have predominantly anion character to crystal orbitals derived from the empty titanium 3d orbitals. The optical absorption that occurs at energies below 2.0 eV (λ > 620 nm) does not originate from excitations across the band gap and merits further comment. The shape of CeTiNO$_2$ optical absorption curve between approximately 2.1 and 1.6 eV is qualitatively different than the other three compounds. Given the location of the Ce^{3+} 4f orbitals in the band gap we hypothesize that the unusual shape of the UV-Vis curve in this region is due to transitions from the Ce 4f orbital into the conduction band. This type of transition has been seen in oxides that contain Ce^{3+}, such as CeVO$_4$.[27]

The upturn seen in absorption spectra of the other three compounds on moving into the infrared region (E < 1.7 eV) is likely of a different origin. The trace amounts of TiN (2 – 4 wt. %, observed in neutron powder diffraction patterns[17]) would lead to some absorption in that region, but for the reasons discussed below we feel this is not the main contributor to the sub-band gap absorptions. A more likely cause of this effect is the presence of low levels of Ti^{3+} in the perovskite phase, which could be explained either by anion vacancies, or by RTiN$_{1+x}$O$_{2-x}$ non-stoichiometry. In fact, the slow fourth decay component in the TRIR study hints at such defects. Sub-band gap absorptions, associated with the presence of small amounts of Ti^{3+}, that extend into the mid-IR have been seen in the TiO$_x$N$_y$F$_z$, system.[28] The upturn of absorbance seen in the low energy side of the absorption spectra increases significantly from LaTiNO$_2$ to PrTiNO$_2$ to NdTiNO$_2$.

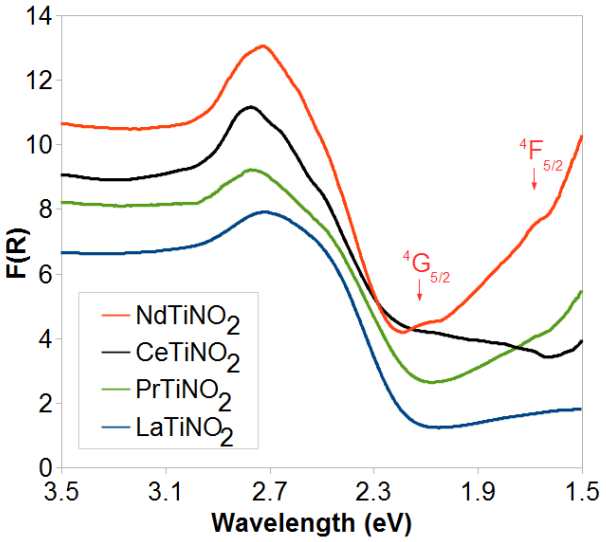

Figure 6. Kubleka-Munk transformed UV-visible diffuse reflectance of RTiNO$_2$. These spectra have not been vertically offset from each other.

In addition to the electronic transitions already discussed, weak features associated with f-f transitions are seen in the NdTiNO$_2$ spectrum. The peaks at 2.1 and 1.6 eV can be assigned to $^4G_{5/2}$ and $^4F_{5/2}$ f-f transitions on Nd^{3+}. Because f-f transitions are forbidden, these transitions are very weak.

3.6 Photocatalytic activity for water oxidation

The photocatalytic O_2 evolution activity for RTiNO$_2$ (R = La, Ce, Pr, Nd) and $SrTiO_3$ samples impregnated with a 2 wt.% CoO_x co-catalyst over a period of eight hours is shown in Figure 7. In these experiments a long pass filter as well as a cold mirror were used so that only visible light (800 nm > λ > 400 nm) reached the photocatalyst. The results of photocatalytic cycling (3×) experiments can be found in the Supporting Information. Trace amounts of nitrogen were detected at the initial illumination onset, which is associated with the removal of surface nitrogen, a typical phenomenon in nitride oxides.[12] The linear rates of O_2 evolution are found to be 17 μmol/g/hr for $LaTiNO_2$, 5 μmol/g/hr for $CeTiNO_2$, 11 μmol/g/hr for $PrTiNO_2$, 16 μmol/g/hr for $NdTiNO_2$, and negligible for $SrTiO_3$.

Prior studies of photocatalytically driven water oxidation by $LaTiNO_2$, with a CoO_x co-catalyst, report a much higher rate of O_2 evolution (~600 μmol/hr).[13] The decrease in activity is owed in large part to the change in lamp wattage (ref. 13 = 300 W; this study = 150 W). For a 300 W Xe arc lamp, power density is typically close to 50 mW/cm^2 (~ 6 suns). Using a Thor Labs Si photodectector, the measured power density of our 150 W Xe lamp was 26 μW/cm^2 (~ 0.5 suns). Differences in the intensity of the light source can have a dramatic effect on photocatalytic evolution rates.[29] At high light intensity (> 150 W or AM1.5), the photocurrent increases are not linear.[30] High photocurrents increase the likelihood of charge transfer from semiconductor to co-catalyst before recombination occurs. This charge separation for water splitting is critical as demonstrated in a homojunction $BiVO_4$/a-Si photoelectrochemical cell.[31] Accounting for this, $LaTiNO_2$ yields results that are in-line with what should be expected from lower power density light. One must also acknowledge that the sample morphologies indicated by SEM and BET are distinct from those mentioned in the investigation of $LaTiNO_2$ by Zhang *et. al.*,[13] another factor that makes direct comparison to that work non-trivial.

The key finding in this paper is relative rates of O_2 evolution for the four oxide nitride photocatalysts studied. In relative terms, the photocatalytic activity order is $LaTiNO_2$ ≈ $NdTiNO_2$ > $PrTiNO_2$ > $CeTiNO_2$. Given the already established behavior of $LaTiNO_2$ as an effective photocatalyst for the oxygen evolution half-reaction, this result shows that $NdTiNO_2$ is equally promising, whereas $PrTiNO_2$ and particularly $CeTiNO_2$ are inferior.

For the most part the variability in the photocatalytic rates of the RTiNO$_2$ compounds studied here is not due to differences in particle size and/or shape, as these compounds have similar surface areas, pore volumes, pore sizes, distributions, and morphologies. Neither is it due to the band gap or the position of the conduction or valence band edges, which are also quite similar across the entire series. Although there may be slight variations in absorption coefficient for each compound, those differences alone cannot explain the differences in photocatalytic activity.

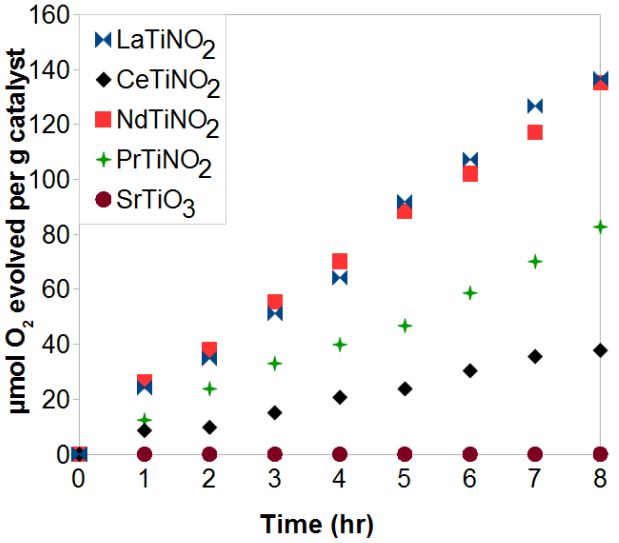

Figure 7. Photocatalytic O_2 evolution for 2 wt. % CoO_x co-catalyst modified compounds RTiNO$_2$ and $SrTiO_3$. 100 mg photocatalyst and 100 mg La_2O_3 (pH buffer) were suspended in 100 mL of a 0.05M $AgNO_3$ solution contained within a closed quartz vessel.

The differences in photocatalytic rates appear to be linked to the presence of partially filled f-orbitals either in the band gap or near the top of the valence band. Because both Ce and Pr have occupied and highly localized 4f states (flat bands) that are energetically accessible to the photogenerated holes this leads to unwanted recombination of the free carriers. In contrast, the 4f orbitals of La^{3+} must lie well above the valence band, and the occupied 4f-orbitals on $NdTiNO_2$ are positioned well below the valence band edge, as shown in Figure 8. Consequently, these two compounds have comparable activities for the oxidation of water.

The recombination of carriers is evidenced by the slow component of the carrier lifetimes in $NdTiNO_2$ (798 ps) and $LaTiNO_2$ (1110 ps), values that are considerably longer than in $PrTiNO_2$ (330 ps) and $CeTiNO_2$ (170 ps). The relatively long carrier lifetime allows carriers enough time to be transferred from the bulk to the surface deposited cobalt co-catalyst, where it then undergoes the cascade of processes that must occur for water oxidation. By proxy, the $PrTiNO_2$ and $CeTiNO_2$ suffer from higher rates of carrier recombination before efficient transfer can occur, directly yielding lower rates of water oxidation.

These results show that prediction or measurement the f-orbital states with respect to the valence band maximum should be part of the process of designing new lanthanoid-containing perovskite nitride oxide photocatalysts. Good candidate compounds should yield f-orbitals that do not fall close to the band edge positions. Many of the heavier rare-earth ions have f-orbital positions known to be more negative than Nd^{3+}.[32] Therefore, compositions such as RTi(N,O)$_x$ (R = Sm, Gd, Ho – Lu) may provide interesting or superior photocatalytic activities because the f-orbitals would reside below the valence band maximum.

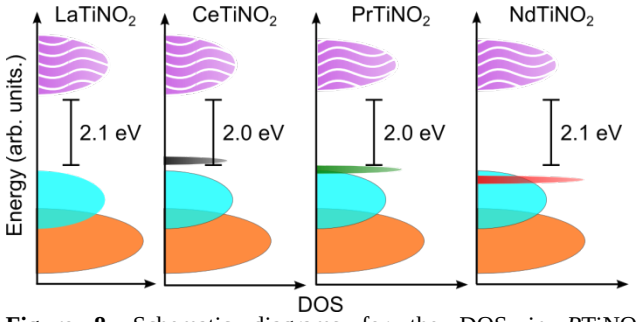

Figure 8. Schematic diagrams for the DOS in *R*TiNO$_2$ perovskites. Orbitals are split into a filled oxygen 2p (orange)/nitrogen 2p (cyan) valence band and an unfilled Ti 3d (wavy violet) conduction band. The localized f-orbital states decrease in energy sequentially for Ce (black), Pr (green), and Nd (red).

It is pertinent to note that LaTiNO$_2$ and NdTiNO$_2$ have similar photocatalytic activities, despite the fact that the latter appears to have a larger concentration of Ti^{3+}. This observation would seem to suggest that while the presence of Ti^{3+} states leads to increased absorption of visible light it does not have a significant impact on the photocatalytic activity. A systematic study on water reduction by the *R*TiNO$_2$ (*R* = Ce – Nd) compounds was not undertaken in this work. However, the electronic data presented here suggests that water reduction results for NdTiNO$_2$ would be similar to those of LaTiNO$_2$, with CeTiNO$_2$ and PrTiNO$_2$ results inferior due to rapid carrier recombination rates.

4. Conclusion

The photocatalytic properties of the *R*TiNO$_2$ (R = Ce – Nd) perovskites have characterized for the first time. The band gaps of all four compounds lie between 2.0 – 2.1 eV, which allow them to absorb a significant fraction of the visible spectrum. When powders of these compounds are impregnated with 2 wt. % cobalt co-catalyst they are capable of photocatalytic water oxidation. The oxygen evolution rates are 5 – 17 μmol/hour/g under illumination from a 150 W Xe arc lamp ($400 < \lambda < 800$ nm), with the activities following the trend: La ≈ Nd > Pr > Ce. XPS measurements show that the 4f-orbitals play a critical role in photocatalytic activity. When they lie near the top of the valence band, as is the case for Ce and Pr, photocatalytic activities decrease because the partially filled 4f orbitals act as recombination centers. TRIR kinetic decays reveal that the Ce and Pr compounds have much shorter carrier lifetimes. The O_2 evolution rates in NdTiNO$_2$ are comparable to LaTiNO$_2$, which makes this compound a candidate for further optimization as a water oxidation photocatalyst and demonstrates the viability of other possible *R*TiNO$_2$ photocatalysts.

ASSOCIATED CONTENT

Supporting Information. BET surface area measurements for *R*TiNO$_2$ (*R* = La, Ce, Nd). TRIR for *R*TiNO$_2$ (*R* = La, Ce, Nd). Full photocatayltic cycling. This material is available free of charge via the Internet at http://pubs.acs.org.

AUTHOR INFORMATION

Corresponding Author

* zhenguo@uow.edu.au; woodward@chemistry.ohio-state.edu

Author Contributions

The manuscript was written through contributions of all authors. All authors have given approval to the final version of the manuscript.

Funding Sources

The Australian Research Council (Discovery Early Career Research Award, DE120101496) is acknowledged for funding. Partial support was supplied by the Center for Emergent Materials at the Ohio State University, an NSF Materials Research Science and Engineering Center (DMR-0820414).

ACKNOWLEDGMENT

The authors would like to thank Dr. Claudia Turro and Dr. Malcolm Chisholm at OSU for access to the TRIR, Dr. Elizabeth Hommel at OSU for assistance with the XPS, Dr. Umit Ozkan and Hyuntae Sohn at OSU for access to and assistance on the BET.

REFERENCES

(1) Kudo,A.; Ueda, K.; Kato, H.; *Catal. Lett.*, **1998**, *53*, 229.
(2) Kudo, A.; Omori, K.; Kato, H.; *J. Am. Chem. Soc.*, **1999**, *121*, 11459.
(3) Tokunaga, S.; Kato, H.; Kudo, A.; *Chem. Mater.*, **2001**, *13*, 4624.
(4) Yu, J.Q.; Kudo, A.; *Adv. Funct. Mater.*, **2006**, *16*, 2163.
(5) Grätzel, M.; *Energy Resources through Photochemistry and Catalysis*, Academic Press, New York, **1983**.
(6) Serpone, N.; Pelizzetti, E.; *Photocatalysis*, Wiley, New York, **1989**.
(7) Krasnovsky, A. A.; Brin, G. P.; *Dokl. Akad. Nauk SSSR*, **1962**, *147*, 656.
(8) Darwent, J. R.; Mills, A.; *J. Chem. Soc., Faraday Trans.* **1982**, *2*, 359.
(9) Chun, W-J.; Ishikawa, A.; Fujisawa, H.; Takata, T.; Kondo, J.N.; Hara, M; Kawai, M; Matsumoto, Y; Domen, K.; *J. Phys Chem B*, **2003**, *107*, 1798.
(10) Hitoki, G.; Takata, T.; Kondo, J.N.; Hara, M.; Kobayashi, H.; Domen, K.; *Chem. Commun.*, **2002**, 1698.
(11) Hara, M.; Nunoshige, J.; Takata, T.; Kondo, J.N.; Domen, K.; *Chem. Commun.*, **2003**, 3000.
(12) Hisatomi, T.; Katayama, C.; Moriya, Y.; Minegishi, T.; Katayama, M.; Nishiyama, H.; Yamada, T.; Domen, K.; *Energy Environ. Sci.*, **2013**, *6*, 3595.
(13) Zhang, F; Yamakata, A.; Maeda, K.; Moriya, Y.; Takata, T.; Kubota, J.; Teshima, K.; Oishi, S.; Domen, K.; *J. Amer. Chem. Soc.*, **2012**, *134*, 8348.
(14) Clarke, S.J.; Guinot, B.P.; Michie, C.W.; Calmont, M.J.C.; Rosseinsky, M.J.; *Chem. Mater.*, **2002**, *14*, 288.
(15) Tessier, F.; Le Gendre, L.; Cheviré, F.; Marchand, R.; Navrotsky, A.; *Chem. Mater.*, **2005**, *17*, 3570.
(16) Ebbinghaus, S.G.; Aguiar, R.; Weidenkaff, A.; Gsell, S.; Reller, A.; *Solid State Sci.*, **2008**, *10*, 709.
(17) Porter, S.; Huang, Z.; Cheng, Z.; Avdeev, M.; Chen, Z.; Dou, S.; Woodward, P.; *J. Solid State Chem.*, **2015**, DOI: 10.1016/j.jssc.2015.01.023.
(18) Toby, B. H.; *J. Appl. Crystallogr*. **2001**, *34*, 210.
(19) Wang, J.; Burdzinski, G.; Kubicki, J.; Platz, M. S. *J. Am. Chem. Soc.* **2008**, *130*, 11195.
(20) Machida, M.; Murakami, S.; Kijima, T.; Matsushima, S.; Arai, M.; *J. Phys. Chem. B*, **2001**, *105*, 3289.
(21) Chun, W. J.; Ishikawa, A.; Fujisawa, H.; Takata, T.; Kondo, J. N.; Hara, M.; Kawai, M.; Matsumoto, Y.; Domen, K, *J Phys Chem B*, **2003**, *107*, 1798.
(22) Llansola-Portoles, M.; Bergkamp, J.; Finkelstein-Shapiro, D.; Sherman, B.; Kodis, G.; Dimitrijevic, N.; Gust, D.; Moore, T.; Moore, A.; *J. Phys. Chem. A.*, **2014**, *118*, 10631.
(23) Le Paven-Thivet, C.; Ishikawa, A.; Ziani, A.; Le Gendre, L.; Yoshida, M.; Kubota, J.; Domen, K.; *J. Phys. Chem. C*, **2009**, *113*, 6156.

(24) Singh, R.B.; Matsuzaki, H.; Suzuki, Y.; Seki, K.; Minegishi, T.; Hisatomi, T.; Domen, K.; Furube, A.; *J. Amer. Chem. Soc.*, **2014**, *136*, 17324.
(25) Shapiro, I.P.; *Optika i Spektroskopiya*, **1958**, *4*, 256.
(26) Kasahara, A.; Nukumizu, K.; Takata, T.; Kondo, J. N.; Hara, M.; Kobayashi, H.; & Domen, K.; *J. Phys. Chem. B*, **2003**, *107*, 791.
(27) Dolgos, M. R; Paraskos, A. M.; Stoltzfus, M. W.; Yarnell, S. C; Woodward, P. M.; *J. Solid State Chem.*, **2009**, *182*, 1964.
(28) Seibel, H. A.; Karen, P.; Wagner, T. R.; Woodward, P. M.; *J. Mater. Chem.* **2009**, *19*, 471.
(29) Hisatomi, T.; Miyazaki, K.; Takanabe, K.; Maeda, K.; Kubota, J.; Sakata, Y.; Domen, K; *Chem. Phys. Let.*, **2010**, *486*, 144.
(30) Ruan, C.; Paulose, M.; Varghese, O.K.; Grimes, C.A. *Solar Energy Mater. Solar* Cells, **2006**, *90*, 1283.
(31) Abdi, F.F.; Han, L.; Smets, A.H.M.; Zeman, M.; Dam, B.; van de Krol, R.; *Nature Comm.*, **2013**, *4*, 2195.
(32) Thiel, C. W.; Cruguel, H.; Wu, H.; Sun, Y.; Lapeyre, G. J.; Cone, R. L.; Macfarlane, R. M.; *Phys. Rev. B*, **2001**, *64*, 085107.

SYNOPSIS TOC.

Spencer H. Porter, Zhenguo Huang,* Shixue Dou, Samantha Brown-Xu, A.T.M. Golam Sarwar, Roberto C. Myers, and Patrick M. Woodward*

Chem. Mater. **2014** XX YYY

Electronic structure and photocatalytic water oxidation activity of RTiNO$_2$ (R = Ce, Pr and Nd) perovskite nitride oxides

Studies of the electronic structure and photocatalytic activity of RTiNO$_2$ (R = Ce, Pr and Nd) perovskites reveal that the relative energies of the R 4f-orbitals play a central role in determining the water oxidation activities. NdTiNO$_2$ is shown to be a promising photocatalyst for the water oxidation half-reaction.

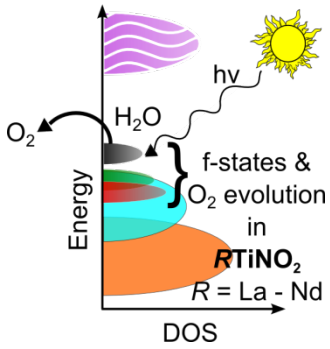

Table of Contents artwork see ^